ADVANCED FUNCTIONAL MATERIALS
www.afm-journal.de

# Nanotransfer Printing of Functional Nanomaterials on Electrospun Fibers for Wearable Healthcare Applications

*Ji-Hwan Ha, Jiwoo Ko, Junseong Ahn, Yongrok Jeong, Jihyeon Ahn, Soonhyoung Hwang, Sohee Jeon, Dahong Kim, Su A Park, Jimin Gu, Jungrak Choi, Hyeonseok Han, Chankyu Han, Byeongmin Kang, Byung-Ho Kang, Seokjoo Cho, Yeong Jae Kwon, Cheolmin Kim, Sunkun Choi, Gi-Dong Sim, Jun-Ho Jeong,* and Inkyu Park**

**With the advancement of functional textile technology, there is a growing demand for functional enhancements in textiles from both industrial and societal perspectives. Recently, nanopattern transfer technology has emerged as a potential approach for fabricating functional textiles. However, conventional transfer methods have some limitations such as transfer difficulties on curved fiber surfaces, polymer residues, and delamination of transferred nanopatterns. In this study, an advanced nanopattern transfer method based on surface modification and thermoforming principles is applied to microscale electrospun fibers. This transfer method utilizes covalent bonding and mechanical interlocking between nanopatterns and the fibers without requiring extra adhesives. Various nanopatterns transferred electrospun fibers possess significant potential for diverse wearable healthcare applications. This work introduces two specific application scenarios in the field of wearable healthcare, both of which leverage the light: diagnostics and antimicrobials. Versatile textile with silver nanogap-pattern detects glucose in sweat, diagnosing hypoglycemia and diabetes by shifting Raman peaks from 1071.0 to 1075.4 $cm^{-1}$ for 0 to 150 μM glucose. Additionally, a bactericidal mask using visible light to induce the photocatalytic degradation effect of titanium dioxide and silver nanopatterns is developed. Bactericidal efficacy against Escherichia coli and Staphylococcus aureus is 99.9% due to photolysis from visible light irradiation.**

## 1. Introduction

Textiles are important materials that can be used in a variety of applications, including clothing for human fashion and protection,[1] and masks to prevent disease infection.[2–4] Textile-based technologies have evolved beyond their traditional role of simply adorning or protecting the body.[1] The emergence of functional textiles has opened up new possibilities for enabling textiles-based displays,[5–7] physical/chemical sensors,[8–14] and healthcare devices.[15–19] The versatility of functional textiles, which can be incorporated into everyday clothing, enhances the quality and convenience of human life. Particularly, recent years have witnessed significant growth in the use of functional textiles for medical clothing applications,[20] including human vital signs monitoring,[15,16,21,22] disease diagnosis,[23,24] and infection prevention.[25,26] Several methods have been suggested for fabricating functional textiles, including the fibrous coating of functional materials,[27–29] fiberization of composites,[30,31] core-shell-shaped fiber

J.-H. Ha, J. Ko, J. Ahn, J. Gu, H. Han, C. Han, B. Kang, B.-H. Kang, S. Cho, Y. J. Kwon, C. Kim, S. Choi, G.-D. Sim, I. Park
Department of Mechanical Engineering
Korea Advanced Institute of Science and Technology
Daejeon 34141, Republic of Korea
E-mail: inkyu@kaist.ac.kr

J.-H. Ha, J. Ko, S. Hwang, S. Jeon, S. A Park, B. Kang, J.-H. Jeong
Nano Lithography and Manufacturing Research Center
Korea Institute of Machinery and Materials
Daejeon 34103, Republic of Korea
E-mail: jhjeong@kimm.re.kr

The ORCID identification number(s) for the author(s) of this article can be found under https://doi.org/10.1002/adfm.202401404

DOI: 10.1002/adfm.202401404

J. Ahn
Department of Electro-Mechanical Systems Engineering
Korea University
Sejong 30019, Republic of Korea

Y. Jeong
Korea Atomic Energy Research Institute (KAERI)
11, Daedeok-daero 989beon-gil, Yuseong-gu, Daejeon 34057, Republic of Korea

D. Kim
Department of Applied Bioengineering
Graduate School of Convergence Science and Technology
Seoul National University
Seoul 08826, Republic of Korea

J. Choi
Electronics and Telecommunications Research Institute (ETRI)
Daejeon 34129, Republic of Korea

 

design,[32–34] and the transfer of nanomaterials and nanopatterns onto fibers.[8] Nevertheless, conventional methods employed in the fabricating of functional textiles have faced certain constraints. These limitations include a heavy reliance on the adhesion properties of coating materials, inconsistent performance due to uneven dispersion of functional fillers within composites, and restrictions on the selection of materials for functional textiles, primarily confined to organic substances.

Nanotransfer printing (nTP) is a simple technique that facilitates the consistent and controllable transfer of nanopatterns of inorganic materials onto various substrates through manipulation of the adhesion between the interface and the transferred target material. Among the functional textile fabrication methods, transferring inorganic (e.g., metals, metal oxides) nanopatterns onto textiles using nTP method has proven challenging. This is largely because of the curved geometry of the fibers and limited interfacial adhesion between the fibers and nanopatterns. A recent study introduced a transfer method that uses a hyaluronic acid-based water-soluble polymer template for transferring metal nano-line patterns onto the curved surface of fibers.[8] In order to achieve reliable transfer of nano-line patterns onto the fibers, traditional fabric materials such as silk, spandex, and cotton were required to have a minimum diameter of 50 μm and exhibit favorable wettability. Despite offering a novel approach to transfer nanopatterns onto fibers, the method still faced several limitations. The challenge arises from attempting to transfer nanopatterns onto fine fibers with small diameters, typically below 10 μm,[8,31,32] with the aim of enhancing textile quality, fit, and reducing roughness. Stable nanopattern transfer on such these fibers have been difficult because of the curved shape, small contact area, and low interfacial adhesion of the fibers. Although certain studies have made efforts to pattern smaller-diameter fibers using nanoscale molds,[35] the utilization of a blend of inorganic materials for functional enhancement in small-diameter fibers has not been reported thus far. Incomplete dissolution of the polymer can leave residuals on the fiber and nanopatterns. Additionally, the absence of additional adhesive can lead to delamination of the transferred nanopatterns by external forces. Furthermore, the curved surface geometry of the fibers and flow of the aqueous solution can impose constraints on the uniformity and pattern shape of the transferred nanopatterns.

To address this issue, this study proposes a straightforward method for transferring metals and metal oxides-based nanopatterns (M/MO NPs) to microscale fibers using the principles of surface modification and thermoforming. The functional textiles developed in this study are made from thermoplastic polyurethane (TPU) fibers using an electrospinning process (ESP) at several microscales to offer greater fit than conventional textiles with larger diameters. In order to facilitate the transfer of M/MO NPs onto electrospun fibers, an oxygen plasma-based surface modification strategy was employed, which yielded two significant effects: mold etching and generation of chemical bonds. This strategy enables the reliable transfer of M/MO NPs onto electrospun TPU fibers without the need for additional adhesives or a water-soluble polymer template. The interfacial adhesion between the electrospun fibers and nanopatterns is improved by the presence of chemical bonds,[36] including covalent and hydrogen bonds. Furthermore, by subjecting the electrospun TPU fibers to specific temperature conditions, applying heat and pressure can be employed to enhance the mechanical interlocking. This phenomenon occurs as the fiber surface deforms its shape when pressed and thermoformed in contact with the nanopatterns. For the optimization of this fabrication strategy, a parametric study on the oxygen plasma exposure time, transfer pressure, and transfer temperature was conducted.

Various transferable nanopatterns based on metals and metal oxides are demonstrated, and wearable healthcare garment applications were developed. This study proposes a diagnosable garment that incorporates 4-mercaptophenylboronic acid (4-MPBA) and silver nanogap patterns. The diagnosable garment has the ability to measure glucose levels in sweat, which correspond to the glucose levels found in individuals with hypoglycemia and diabetes. In addition, a photocatalytic bactericidal mask composed of electrospun TPU fibers integrated with transferred $TiO_2$-Ag-$TiO_2$ (TAT) nanopatterns was suggested. The experimental results show the mask's capability to induce photocatalytic degradation, leading to the eradication of bacteria upon exposure to visible light irradiation.

## 2. Result and Discussion

### 2.1. Research Strategy and Concept

Despite previous efforts to fabricate composite fibers using a combination of inorganic materials and polymers for the production of functional fibers in functional textiles, composite fiber fabrication has faced limitations due to challenges related to filler material aggregation and phase separation between the inorganic and polymer components. Moreover, several limitations exist in the water-soluble template-based nanotransfer printing of M/MO NPs[8] including the nanopatterns misalignment during the template transfer process by solvent, surface contamination resulting from residual materials after transfer process, and delamination caused by insufficient interfacial bonding between the fibers and the M/MO NPs. To overcome these limitations, we propose to combine electrospun thermoplastic polyurethane (TPU) composite fibers with M/MO NPs through surface modification and heat pressing in this study. This approach eliminates the need for extra dispersion and solvent processes, offering a potential solution to the previously encountered challenges such as aggregation of nanomaterials and residual polymers. Furthermore, our proposed process facilitates the fabrication of composite functional fibers by integrating a mixture of materials, thereby creating a hierarchical structure that spans from the microscale to the nanoscale. This multiscale complexity can be applied to bioinspired applications for wearable healthcare applications.[37] Within the scope of this study, we have developed the electrospun fibers with M/MP NPs into the wearable healthcare applications.

**Figure 1a** depicts fabrication strategies aimed at surmounting the previously highlighted challenges in transferring and integrating nanopatterns onto electrospun fibers. Electrospinning was employed to achieve micro-scale fiberization of TPU. The objective was to leverage the thermoforming capabilities of TPU through heat pressing, ensuring a substantial area conducive to the stable transfer of various nanopatterns. Nanopatterned molds of polyurethane acrylate (PUA) are fabricated using the nanoimprint technique, and target materials such as metals or metal oxides are deposited onto the surface via the E-beam deposition

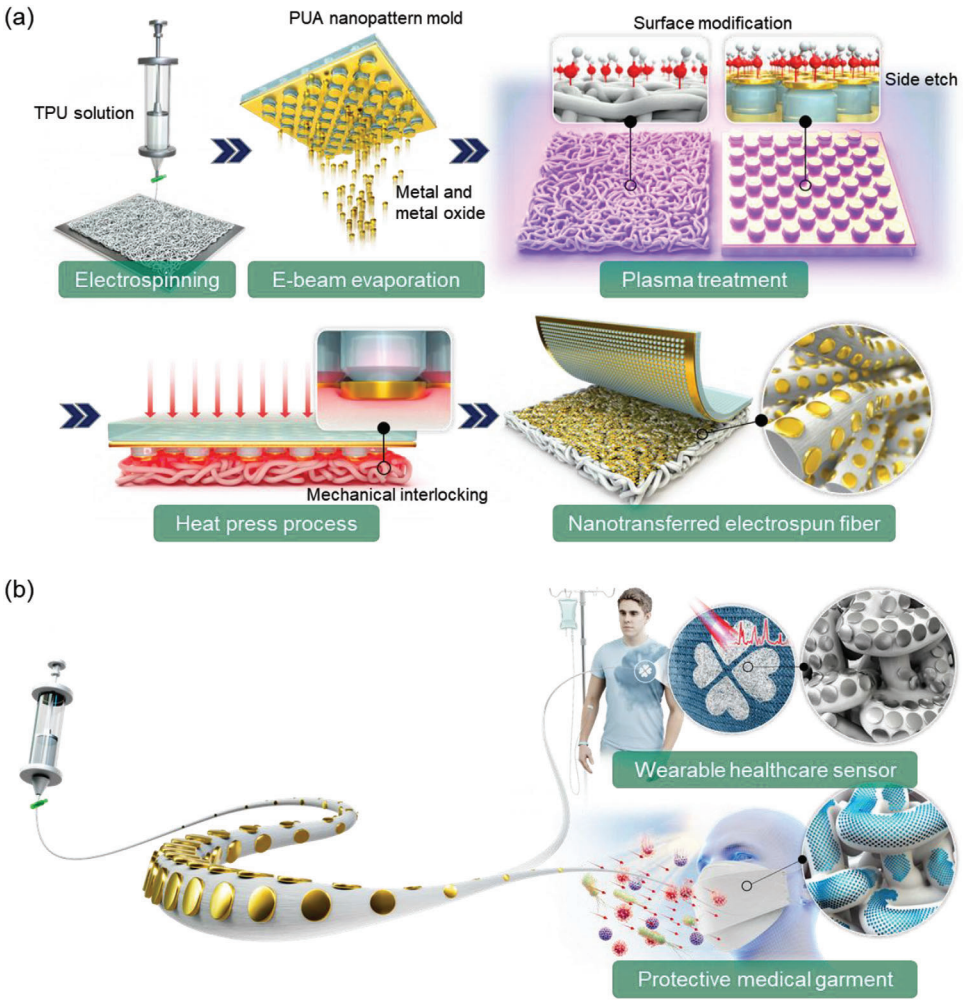


**Figure 1.** a) Schematic shows fabrication strategies for transferring nanopatterns onto electrospun fibers. The process involves oxygen plasma treatment of electrospun TPU fibers and M/MO NP molds using the nano imprinting lithography process and E-beam deposition. Subsequently, the nanopatterns are transferred via a heat pressing process. Finally, electrospun fibers with transferred M/MO NPs are fabricated. b) Schematic representation of the research overview. Fabrication of the microscale TPU fiber by ESP and oxygen plasma treatment to improve the adhesion forces. Transfer of the various rationally designed-M/MO NPs to the electrospun TPU fibers. Application 1: The wearable SERS-based sweat sensor patch containing the nanocircular Ag pattern-transferred TPU fibers is attached to general clothing to diagnose diabetes by measurement of the sweat glucose concentration. iv) Application 2: A bactericidal mask containing the TAT nanodot pattern-transferred TPU fibers exhibits bactericidal performance in the visible light region.

method. Subsequently, oxygen plasma treatment is conducted, a pivotal step in the suggested fabrication strategies. Previous research suggests that to enhance the stability of the metal nanopattern transfer procedure, one should reduce the adhesive forces between the mold and nanopatterns ($F_{\text{mold}}$) and simultaneously increase the adhesive forces between the target substrate and the nanopatterns ($F_{\text{substrate}}$) like Equation (1).[38]

$$F_{substrate} - F_{mold} > 0 \quad (1)$$

This oxygen plasma treatment-based strategy presents an enhanced approach whereby stable M/MO NPs are transferred onto electrospun fibers through a combination of surface modification such as hydroxyl group formation and surface energy increasing, which increases the $F_{\text{substrate}}$, and the etching of the mold materials, which decreases $F_{\text{mold}}$. In particular, when the bonding forces between the M/MO NPs and the target substrate ($F_{\text{substrate}}$) are larger than those between the M/MO NPs and the mold ($F_{\text{mold}}$) by partially etching the mold underneath the M/MO NPs, the transfer quality can be dramatically improved. The secondary pivotal step, heat pressing, is utilized to transfer nanopatterns onto the electrospun fibers. In this process, the transfer stability can be further enhanced by causing mechanical interlocking (increment in $F_{\text{substrate}}$) between the M/MO NPs and the TPU fibers during heat pressing. Due to the thermoforming properties of TPU, during the heat pressing phase, the TPU fibers deform to the structure of the nanopatterns, bolstering the adhesion between the nanopatterns and the TPU. This enhancement can be attributed to the thermoforming characteristic of the TPU polymer, which allows for effective binding within the temperature range between its melting point ($T_m$) and glass transition temperature ($T_g$).[39] Following these procedures, the PUA mold is

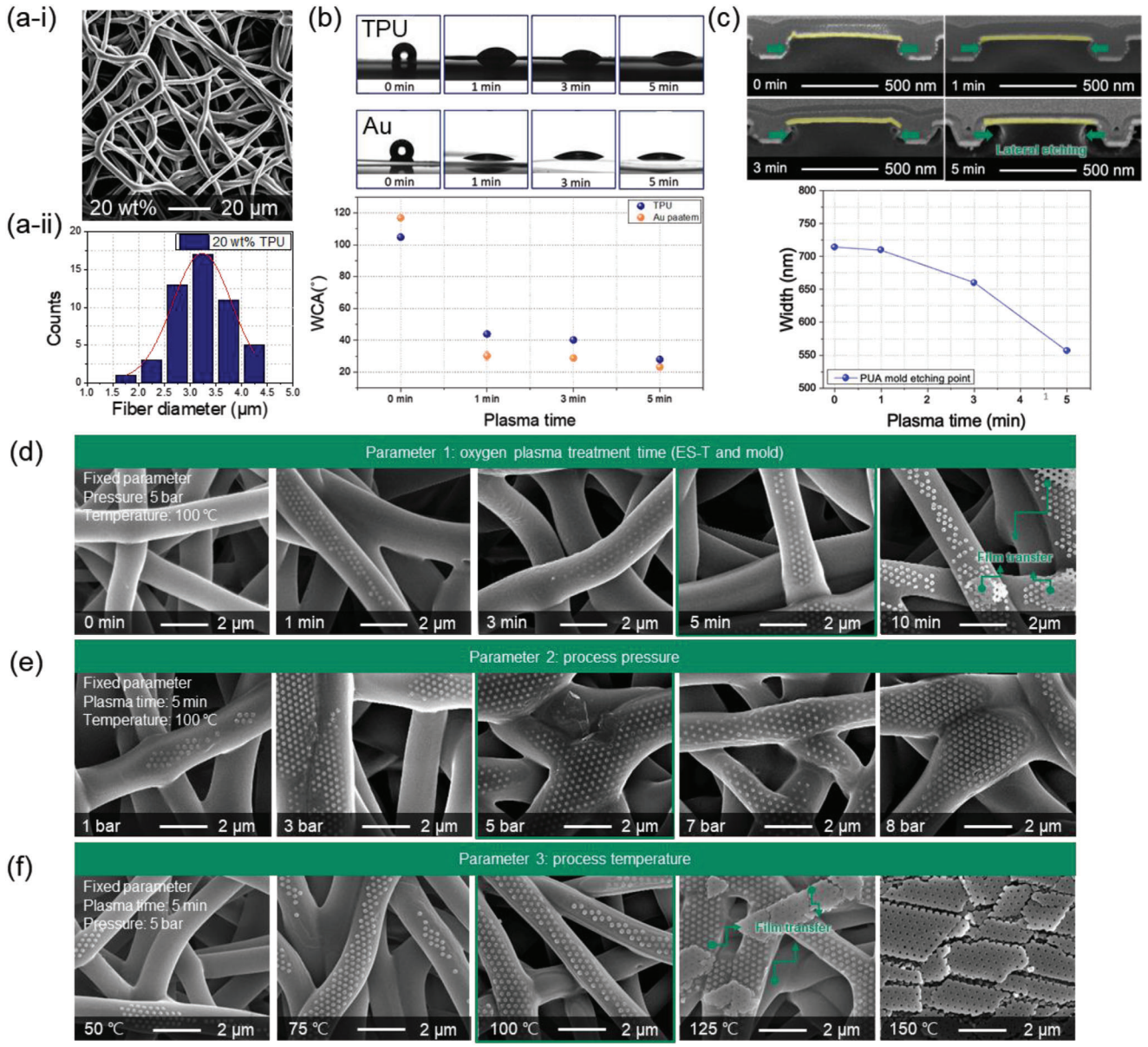


**Figure 2.** a) Examination of the morphological properties of the electrospun TPU fibers by i) SEM and ii) a diameter distribution plot. The electrospun TPU fibers exhibited a size distribution of 1.5–4.5 μm. b) Surface modification results obtained for the electrospun TPU sheet and the metal evaporation-patterned film after different oxygen plasma treatment times. c) FIB images of the Au evaporated-nanopatterned PUA molds following different oxygen plasma treatment times. The etching area of the mold was increased by increasing the oxygen plasma treatment time. Variation in the morphological properties of the gold nanodot pattern-transferred electrospun TPU fibers at different d) oxygen plasma treatment times, e) pressures, and f) temperatures.

detached, resulting in electrospun fibers with the nanopatterns transferred onto them.

Figure 1b illustrates an overview of the potential applications of the M/MO NPs transferred electrospun fibers. While nanopatterns transferred electrospun fibers have the potential for diverse industrial applications, this particular study focused on their utilization in wearable healthcare applications. Specifically, these fibers-based textiles were employed for purposes such as glucose level monitoring and the photocatalytic bactericidal mask under visible light.

### 2.2. Parametric Study of M/MO NPs Transfer onto the Electrospun Fibers

Prior to the optimization of the M/MO NP transfer process, it was necessary to confirm the basic properties of the TPU fibers prepared by ESP. As shown in **Figure** 2a, the diameters of the electrospun fibers distributed from 1.5 to 4.5 μm when highly viscous 20 wt.% TPU solution was used. The morphological characteristics of the fibers, produced using various concentrations of TPU solution, are shown in Figure S1 (Supporting Information).

It is evident that employing a 15 wt.% TPU solution with lower viscosity resulted in fibers with diameters ranging from 0.5 to 2.5 µm. In addition, electrospinning a 10 wt.% TPU solution led to the creation of fibers with diameters less than 1 µm. However, it should be noted that in the latter case, numerous beads were also formed since the low viscosity of the solution led to an instability during the electrospinning process. Since such beads and nanoscale diameter of the electrospun fibers can reduce transfer quality, electrospun fibers using a 20 wt.% TPU solution were employed to facilitate high-quality transfer of M/MO NPs. FTIR analysis confirmed that the electrospun fibers were composed of TPU materials (Figure S2, Supporting Information). A urethane peak was identified in the range of 1727–1698 $cm^{-1}$, and a polyester peak was discerned between 1168 and 1074 $cm^{-1}$. In order to optimize the transfer of the enhanced M/MO NPs, it was crucial to assess both the surface modification achieved through oxygen plasma treatment and the etching properties of the molds. Following surface modification of the TPU fibers by oxygen plasma treatment, water contact angles (WCA) were observed. More specifically, as shown in Figure 2b, WCA analysis is presented for the gold-deposited nanopattern mold and the electrospun TPU according to the treatment time. The results indicated that increasing the plasma treatment time from 0 to 1, 3, and 5 min resulted in a reduction in the WCA for both TPU and gold-deposited nanopattern mold surfaces. Specifically, the WCA values were as follows: TPU (0 min = 104.8°, 1 min = 43.9°, 3 min = 40.2°, 5 min = 27.9°) and Au (0 min = 117°, 1 min = 30.2°, 3 min = 28.8°, 5 min = 23.2°). The decrease in WCA observed after oxygen plasma treatment can be attributed to the increase in surface energy caused by the treatment, as reported in previous studies.[40–42] The plasma treatment leads to the generation of hydroxyl groups on the surface, which enhances the adhesion between different interfaces. Moreover, during heating, these hydroxyl groups can facilitate the formation of covalent bonds, further strengthening the interfacial adhesion. Furthermore, the −NH groups present in the urethane composition of TPU can form hydrogen bonds with the -OH groups emerging on the nanopatterned surface.[43,44] Figure S3 (Supporting Information) shows the changes in hydroxyl group (3400–3600 $cm^{-1}$) volume in electrospun TPU and Au nanopatterns as a function of plasma treatment time. It also shows the increase in urethane group (1570–1760 $cm^{-1}$) volume resulting from the covalent bonding between hydroxyl and isocyanate groups (2250–2270 $cm^{-1}$) due to the heat pressing process. As depicted in Figure S4 (Supporting Information), the XPS analysis of electrospun TPU before and after the nanopattern transfer process identified consistent peaks of C1s, O1s, and N1s. Following the transfer of Au nanopatterns onto electrospun TPU, an additional Au4f peak observed, highlighting the successful transferring Au nanopatterns. Furthermore, a notable reduction in isocyanate groups was observed, indicative of covalent bonding occurring as a result of the nanopattern transfer. Therefore, the fabrication of electrospun TPU fibers with M/MO NPs can yield enhanced transfer quality, attributable to the increased $F_{substrate}$. This oxygen plasma treatment not only increases $F_{substrate}$ through surface functional group formation but also reduces $F_{mold}$ by etching the base mold. In the following Figure 2c, the results of the etching aimed at reducing the $F_{mold}$ from a morphological perspective are presented. Cross-sectional morphology analysis utilizing a focused ion beam (FIB) was conducted to validate the pattern width of the PUA-based mold (Figure S5, Supporting Information), which exhibited a gradual decrease with increasing plasma treatment time. This analysis provided empirical evidence of the mold's pattern width decreasing according to the increased plasma treatment time. Consequently, the PUA mold, which initially had a square nanopattern width of 720 nm, exhibited pattern widths of 715, 663, and 556 nm after 1, 3, and 5 min of plasma treatment, respectively.

The morphologies of nanopatterns transferred onto electrospun fibers by varying the transfer parameters (plasma processing time, temperature, and pressure) are shown Figure 2d–e. As observed in Figure 2d, the amount of stably transferred M/MO NPs increased with a longer plasma treatment time at 100 °C and 5 bar pressure (fixed condition) owing to the higher surface energy, formation of surface functional groups on the surface, and reduced $F_b$ by the reduction of mold area beneath the M/MO NPs. However, when the plasma treatment time was further increased to 10 min, the whole deposited Au film on the mold (pattern and bottom film) was transferred onto the electrospun fibers. By varying the pressure (Figure 2e), a significantly higher degree of M/MO NP transfer was observed at 5 bar compared to at 1 and 3 bars. In addition to achieving stable nanopatterns transfer characteristics depending on the degree of contact with the surface of the electrospun fiber, a pressure of 5 bar also led to an optimal pattern transfer. It was observed that pressures exceeding 5 bar (specifically 7 and 8 bars) did not result in an increase in the number of transferred nanopatterns. In addition, the effect of process temperature was investigated. Figure 2f shows the results of nanopattern transfer according to process temperature. At 50 °C, the transferred nanopatterns exhibit notably reduced quality, as the process temperature is beneath the $T_g$ of the TPU, not expressing its thermoforming capabilities. The results of the transfer conducted at 50 °C revealed that there were emptier and smooth fiber surfaces observed, rather than areas where the M/MO NPs were successfully transferred. Under the elevated temperature condition at 75 °C, the amount of transferred M/MO NPs increased. However, empty fiber surfaces without M/MO NPs were still observed. In contrast, at a process temperature of 100 °C, the M/MO NPs were stably transferred onto the contact surface of the electrospun fiber. Nevertheless, when subjected to elevated process temperatures (specifically, 125 and 150 °C), the viscosity of TPU decreased due to the temperature increase. This resulted in excessive transfer of the metal film due to mechanical distortion and an increase in the depth of mechanical interlocking within the nanopattern. Based on the above results, the fabrication of M/MO NPs with electrospun fiber was optimized (plasma treatment time: 5 min, process temperature: 100 °C, and process pressure: 5 bar). Figure S6 (Supporting Information) shows the M/MO NPs transferred electrospun fibers and the PUA mold after the nanotransfer process. The nanopattern transferred area was determined using Image J software,[45] resulting in a calculated percentage of nanopatterns transferred onto the electrospun fibers of 70.8%. For the PUA mold, the percentage of transferred nanopatterns compared to the total nanopatterns was calculated to be 71.6%. These results are attributed to the porosity of the electrospun fiber textile, which leads to non-contact areas during the transfer process.

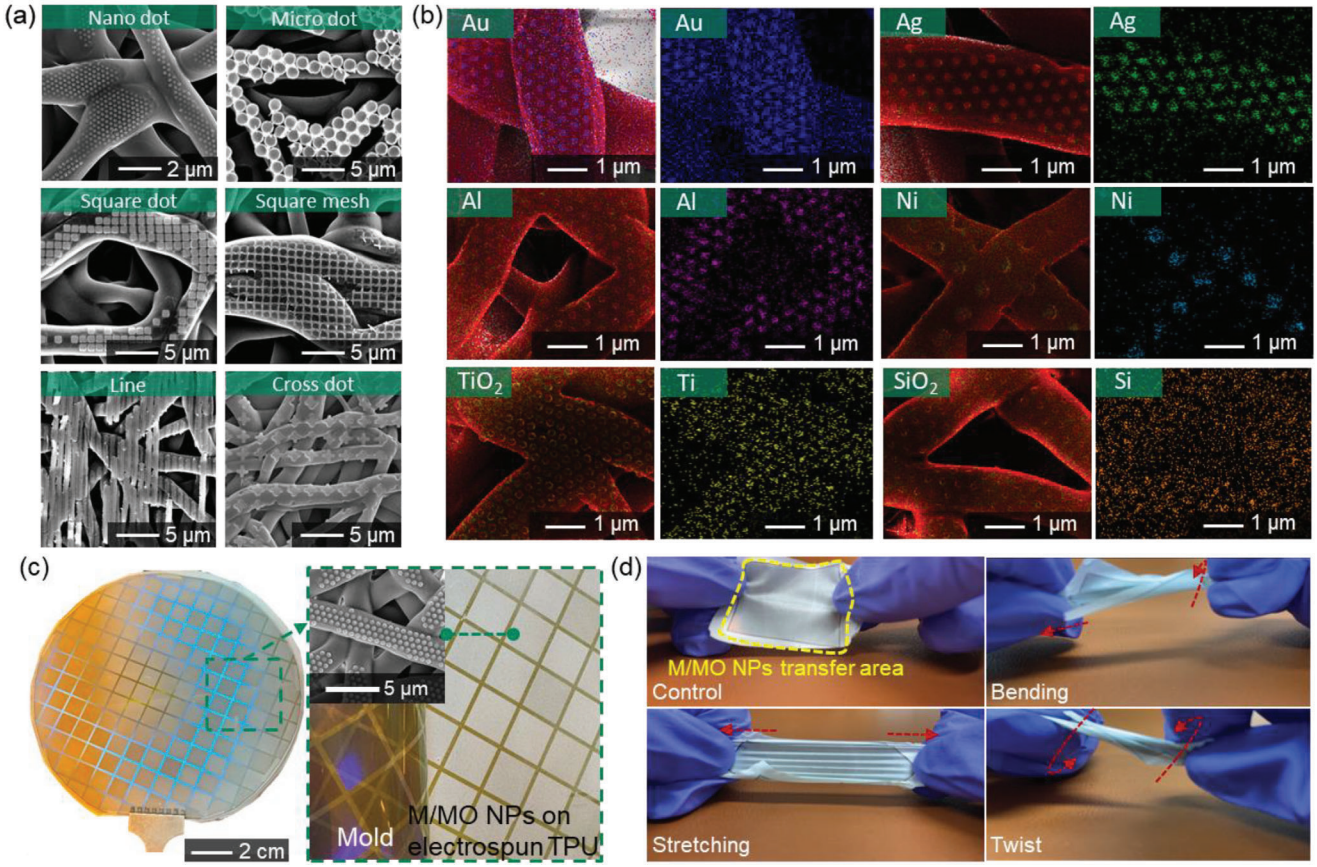


**Figure 3.** a) Images of the prepared nano/micropatterns transferred to the electrospun TPU fiber. b) Transfer of various metal/metal oxide nanodot patterns, as observed by EDS. c) Real camera image of the large area (6 inch) M/MO NPs on the electrospun TPU showing the transfer quality of the M/MO NPs. d) Photographic images of the M/MO NPs on the electrospun TPU wherein different motions are demonstrated to indicate the potential of this system for use in wearable applications.

The proposed strategy allows the transfer of M/MO NPs including various materials as well as patterns of various shapes and scales (i.e., micro- and nanoscales), and the simplicity of this process renders it potentially applicable to a wide range of applications. **Figure** 3a shows the results demonstrating successful transfer of M/MO NPs with various scales and patterns on electrospun TPU fibers. Considering the aspect of transferring patterns across different scales, the capability of pattern transfer was exhibited by effectively transferring circular dot patterns at both the microscale (with a diameter of 1.45 μm) and the nanoscale (with a diameter of 150 nm). Moreover, in terms of encompassing diverse shapes, this was substantiated through the successful transfer of a range of patterns, including square dots (with a width of 800 nm), square meshes (with a width of 800 nm), lines (with a width of 800 nm), and cross dots (with a length of 1200 nm). The successful transfer of various materials was also validated by energy-dispersive X-ray spectroscopy (EDS) analysis, which confirmed the transferability of various materials onto the electrospun TPU fibers, as shown in Figure 3b. Consequently, successful transfer of nanodot patterns composed of metallic materials such as gold, silver, aluminum, and nickel were observed. Owing to their distinctive optical and biological characteristics, the transfer of such metal-based nanopatterns holds potential for application in optical fields, such as color filters[38] and nanophotonic devices,[39] as well as in biological contexts.[46] Titanium dioxide ($TiO_2$) and silicon oxide nanodot patterns were also successfully transferred on the electrospun TPU fibers using the developed method, providing patterns for use in biological applications (e.g., bactericidal films) or battery application owing to their photocatalytic characteristics and electrochemical reduction performances. While the transfer of M/MO NPs can encompass a variety of shapes and materials, its application is constrained by the transfer area. This emphasizes the significance of employing a technique like ESP to create sufficiently expansive electrospun fiber sheets. Furthermore, this process enables the production of large area electrospun TPU fibers with M/MO NPs transferred. ESP is already widely used for large-area production of fiber sheets in various industrial applications. In order to assess the viability of fabricating sizable electrospun TPU fiber sheets embedded with M/MO NPs, experiments were conducted to transfer the nanoparticles onto fiber sheets measuring 6 inches in diameter. Figure 3c shows the results obtained following the transfer of M/MO NPs ($TiO_2$ nano dot patterns) onto the 6-inch wafer-scale electrospun TPU fibers. As can be seen from this figure and Figure S7 (Supporting Information), large-area patterns were stably transferred. Furthermore, multiple patterns of different sizes were successfully combined on a single extensive electrospun fibers, as shown in Figure S8 (Supporting

Information). This involved transferring a high-performance Al-based color filter pattern onto a flexible electrospun TPU substrate of significant area. The resulting textile showcased a color filter effect due to four distinct nanodot pattern types, resulting in hues such as sky blue, green, orange, and purple. These colors were achieved through varying reflectance, a consequence of the diverse nanodot pattern sizes and designs, upon illumination. Figure 3d shows the flexibility and stretchability of the electrospun TPU fibers with M/MO NPs. These characteristics can be attributed to the excellent elasticity of TPU itself, as well as the structure of the textiles composed of numerous bundled fibers. Furthermore, Figure S9 (Supporting Information) shows mechanical properties of fabric and electrospun TPU. The maximum strain, maximum stress, and Young's modulus of electrospun TPU are 671%, 38.4 and 0.022 MPa, respectively (30%, 27.8 and 0.22 MPa, respectively, for cotton fabric). For the wearable application of nanopattern transferred electrospun TPU, the effect of sweat on mechanical properties was observed. Figure S8 (Supporting Information) depicts the mechanical performance evaluation of Au nanopattern transferred electrospun TPU immersed in artificial sweat (pH 5.5, ISO 105-B07) for one day. After immersion, maximum strain of 709%, maximum stress of 33.1 MPa, and Young's modulus of 0.027 MPa were observed, indicating no significant change in mechanical properties by artificial sweat exposure. Figure S11 (Supporting Information) shows the morphology of the nano-transferred electrospun TPU both before and after being subjected to tension (strain: 0%, 50%, 100%, and 200%). The SEM images confirm that the nanopatterns remain firmly attached and do not delaminate when tension is applied. Furthermore, the nanodot pattern's spacing and geometry remained well-preserved even after the wearable system underwent a 50% strain and was subsequently restored (Figure S12, Supporting Information). Video S1 (Supporting Information) displays the in situ SEM result of electrospun TPU with M/MO NPs subjected to 100% strain. It clearly demonstrates that the Au nanopatterns can undergo stretching without experiencing delamination, highlighting the robustness of the nanopattern adhesion. Figure S13 (Supporting Information) shows the adhesion strength of electrospun TPU with M/MO NPs attached to a commercial cotton fabric to ensure versatility for wearable applications. Peel tests between the cotton fabric and electrospun TPU using a commercial fabric bond revealed an adhesion strength of 0.66 N/mm. However, upon attaching the electrospun TPU with M/MO NPs and cotton fabric using the heat pressing adhesion process with oxygen plasma treatment, the adhesion strength was significantly improved to 1.88 N $mm^{-1}$, representing a remarkable 284% improvement. This resilience underscores the exceptional mechanical properties and recovery capabilities of the electrospun TPU in our design. The water-resistant characteristics of electrospun TPU fibers featuring transferred nanopatterns also render them apt for wearable applications. Furthermore, Figure S14 (Supporting Information) shows the nanopattern retention properties in diverse washing conditions. The nanopatterns adhere securely to the TPU fibers without experiencing delamination when subjected to a spinning speed of 1500 rpm without any detergent and speed of 1500 rpm with a commercial pH-neutral detergent, equivalent to condition of a standard washing machine, for a duration of 3 h. After increasing the speed to 3000 rpm for 3 h, only slight delamination of the nanopatterns was observed. During the washing process using flowing water without any detergent, there was no observed delamination of the nanopatterns. In Figure S15 (Supporting Information), SEM images depict the morphologies of nanopattern-transferred electrospun TPU under varying humidity conditions (40% RH, 70% RH, and 98% RH). It is evident that the geometries of the nanopattern transferred electrospun fibers are well-maintained without any delamination of the nanopatterns. These characteristics make them suitable as functional materials for a wide range of wearable systems. Figure S16 (Supporting Information) shows the air permeability of electrospun TPU before and after the transfer of nanopatterns. The results show that electrospun TPU exhibited an air permeability of 5.32 $cm^3/cm^2/s$, while electrospun TPU with nano-patterns, subjected to heat pressing process, showed a slightly reduced air permeability of 2.69 $cm^3/cm^2/s$. The decrease in porosity due to the heat pressing process led to a reduction in air permeability. Nevertheless, it still demonstrated higher air permeability compared to the TPU film (0.03 $cm^3/cm^2/s$) and exhibited air permeability similar to denim fabric (3.41 $cm^3/cm^2/s$). This technique's ability to transfer nanopatterns onto electrospun fibers extends beyond TPU to include other thermoplastic polymers, showcasing its broad applicability. Figure S17 (Supporting Information) illustrates this versatility through both a photograph and SEM images, which depict Au nanopatterns successfully transferred onto electrospun polyvinylalcohol (PVA) and polyvinylidene fluoride (PVDF) fibers. This expansion in the range of compatible polymers significantly enhances the technique's utility, allowing for both nanopattern and polymer selection to be tailored according to specific application requirements. Such adaptability is anticipated to open new avenues in the development of advanced materials, offering customized solutions across various fields of wearable healthcare application.

### 2.3. Application 1: Non-Invasive Diagnosable Garment Using SERS for Sweat Glucose Level Monitoring

The conventional method of glucose monitoring requires the collection of blood from an individual to measure their blood sugar levels.[47] While blood glucose levels have traditionally been employed to diagnose conditions like diabetes and hypoglycemia, the method of blood extraction can be inconvenient. In certain instances, particularly for patients who need frequent glucose level monitoring, such as those with needle phobia, this process can be intimidating and burdensome. Frequent blood collection from a patient for measurement of the blood glucose level of diabetes may result in side effects including anemia and tiredness. Continuously, there has been a pursuit to develop non-invasive methods for measuring glucose levels, aiming to provide patients with a more convenient and comfortable means of monitoring their sweat glucose levels without the need for blood extraction.[48–50] Table S1 (Supporting Information) outlines previously reported glucose measurement methods, glucose measurement concentration ranges, and sensor materials related to wearable glucose sensors in the existing literature. This study, which is specifically aimed at measuring glucose concentrations in sweat, is positioned among these research efforts. Sweat is an inherently complex biomaterial, composed of a diverse substances

including lactate, $Cl^-$, and $Na^+$, among others.[51,52] Furthermore, the glucose concentration within human sweat exhibits subtle variations that are closely linked to an individual's health status. Glucose is a crucial component in the complex makeup of sweat and plays a significant role in diagnosing diseases such as diabetes and hypoglycemia. Glucose level measurement using SERS can act as a reliable indicator of human health status. To showcase the potential for non-invasive diagnostic applications of electrospun TPU fibers containing M/MO NPs, a wearable diagnostic garment was developed for the purpose of monitoring micro-concentration glucose levels in sweat. Given the requirement to detect exceedingly low concentrations of glucose (below 150 µM, corresponding to the sweat glucose concentration in individuals with diabetes),[44] a circular silver (Ag) pattern immobilized with 4-MPBA was devised. This system was subsequently employed to detect glucose levels below 150 µM using the Surface Enhanced Raman Spectroscopy (SERS) method (**Figure 4a**). Upon glucose binding to Ag atoms immobilized with 4-MPBA, a shift in the vibrational structure is triggered. This alteration results in a variation in the Raman shift peak, which is dependent on the glucose concentration (Figure S18, Supporting Information). Through the analysis of these alterations in the Raman spectrum, it becomes feasible to quantitatively determine the glucose concentration in a non-invasive manner. In this study, the glucose level monitoring by SERS was applied to the nanogap between the Ag nanopatterns transferred on electrospun TPU fibers. The hydrophilicity, air permeability, and biocompatibility of the electrospun TPU fibers contribute to making it a comparatively comfortable material suitable for wearable diagnostic applications. As presented in Figure 4b, the biocompatibility of the electrospun TPU fibers was evaluated based on the proliferation rate of fibroblast cells over time (up to 7 days). The cell proliferation morphologies are shown in Figure 4c, wherein the SEM image recorded after 7 days shows that the fibroblasts proliferated broadly over the surface of the electrospun TPU fibers. As shown in Figure 4d, the electrospun TPU fibers including silver nanogap patterns were integrated into a garment as a clover-shaped SERS patch. It should be noted here that due to the specific thermal properties (low $T_g$ and high $T_m$) of the TPU material, it was possible to attach this SERS patch to a range of fabrics (e.g., cotton, silk, spandex, and polyester) by applying heat and pressure. Figure 4e shows an SEM image of the morphology of the SERS patch surface, wherein the diameter and spacing of the circular Ag patterns are 1.44 µm and below100 nm, respectively. Figure 4f shows the measurement result of the glucose concentration of ≤150 µM, corresponding to the range of glucose concentrations present in sweat. More specifically, in the absence of glucose (i.e., 0 µM), a sharp Raman peak at 1071.02 $cm^{-1}$ was observed. Upon increasing the glucose concentration to 10, 30, 50, 100, and 150 µM, the molecular vibration structure of MPBA changed, and the Raman peak shifted to 1071.90 $cm^{-1}$, 1072.78 $cm^{-1}$, 1073.65 $cm^{-1}$, 1074.53 $cm^{-1}$, and 1075.44 $cm^{-1}$ (Figure 4g). For initial glucose concentrations below 50 µM, a notable shift in the Raman peak was observed, which readily indicated the presence of hypoglycemia (≤50 µM). Furthermore, the utilization of Raman shift analysis with the SERS patch allows for the differentiation of glucose levels exceeding 150 µM, thus conferring the capability to diagnose diabetes. Consequently, the implementation of this system is anticipated to facilitate the non-invasive daily monitoring of both diabetes and hypoglycemia. Moreover, it holds the potential to provide relief to patients by eliminating the need for repeated blood collection, while also enabling swift diagnoses of this increasingly prevalent condition.

### 2.4. Application 2: Photocatalytic Bactericidal Mask Using Electrospun Fibers with TAT

Previously, numerous studies have shown that low-cost and non-toxic $TiO_2$-based nanomaterials are able to inhibit the microbial[53,54] and to purify organic/inorganic wastewater[55] through semi-permanent photocatalytic degradation by reactive oxygen.[46] However, $TiO_2$ photocatalysts have limitations such as a poor quantum efficiency, a broad bandgap energy (3.2 eV), and a relatively high electron–hole recombination rate. To prolong the charge carrier lifetime and to achieve the desired bandgap tuning, $TiO_2$ must be increasingly doped with metals such as Ag,[53] which can in turn be used to tune the physicochemical characteristics of this material (i.e., crystallinity and optical properties). As an alternative application, it was considered that the electrospun fiber-based functional textile could be applied as a bactericidal mask under visible light irradiation upon careful transfer of some metal oxides (e.g., $TiO_2$), as outlined in **Figure 5a**. We propose the use of a textile composed of electrospun TPU fibers decorated with TAT for the development of medical garments with bactericidal and purifying capabilities against organic and inorganic contaminants. Due to the high porosity, outstanding stretchability, and low surface roughness of the electrospun TPU mask, this material provides stable and comfortable wearing conditions. The mask with transferred TAT nanopatterns (nanodot patterns diameter: 260 nm, TAT thickness: 70 nm; TPU fiber diameter: 1–3 µm) is anticipated to provide protection against microbes. This is attributed to the enhanced optical attributes of Ag and the antimicrobial potential of $TiO_2$, particularly under visible light exposure. As a result, this design yields protective attire with enhanced antimicrobial and bactericidal capabilities. Figure 5b depicts photographic images of the manufactured mask, while Figure 5c illustrates the SEM-EDS image of electrospun TPU fibers containing TAT nanopatterns. It is evident from the image that the pattern consists of $TiO_2$ and Ag. In this study, a particular configuration involving layers of $TiO_2$ (with a thickness of 30 nm), followed by Ag (with a thickness of 10 nm), and then another layer of $TiO_2$ (with a thickness of 30 nm), was employed. The compositional ratio of TAT is derived from prior studies,[56,57] aiming to identify the ratio that effectively reduces the photoexcitation activation energy and maximizes the generation of OH radicals. This configuration was confirmed by EDS mapping, as shown in Figure S19 (Supporting Information). To evaluate the protection effectiveness of this medical garment (mask), filtration efficiency tests were performed for NaCl, paraffin oil, and bacteria (*Staphylococcus aureus, S. aureus*). As shown in Figure 5d, filtration efficiencies of 66.0% and 71.6% were obtained for NaCl and paraffin oil, respectively. Specifically, the bacterial filtration efficiency (BFE) of this textile against *S. aureus* was 99.5%, thereby demonstrating its superior filtration ability (**Table 1**). Compared to commercial medical masks with BFE ≈95%, the proposed mask exhibited a remarkable bacterial filtration performance. Furthermore, the TAT nanodot-transferred electrospun

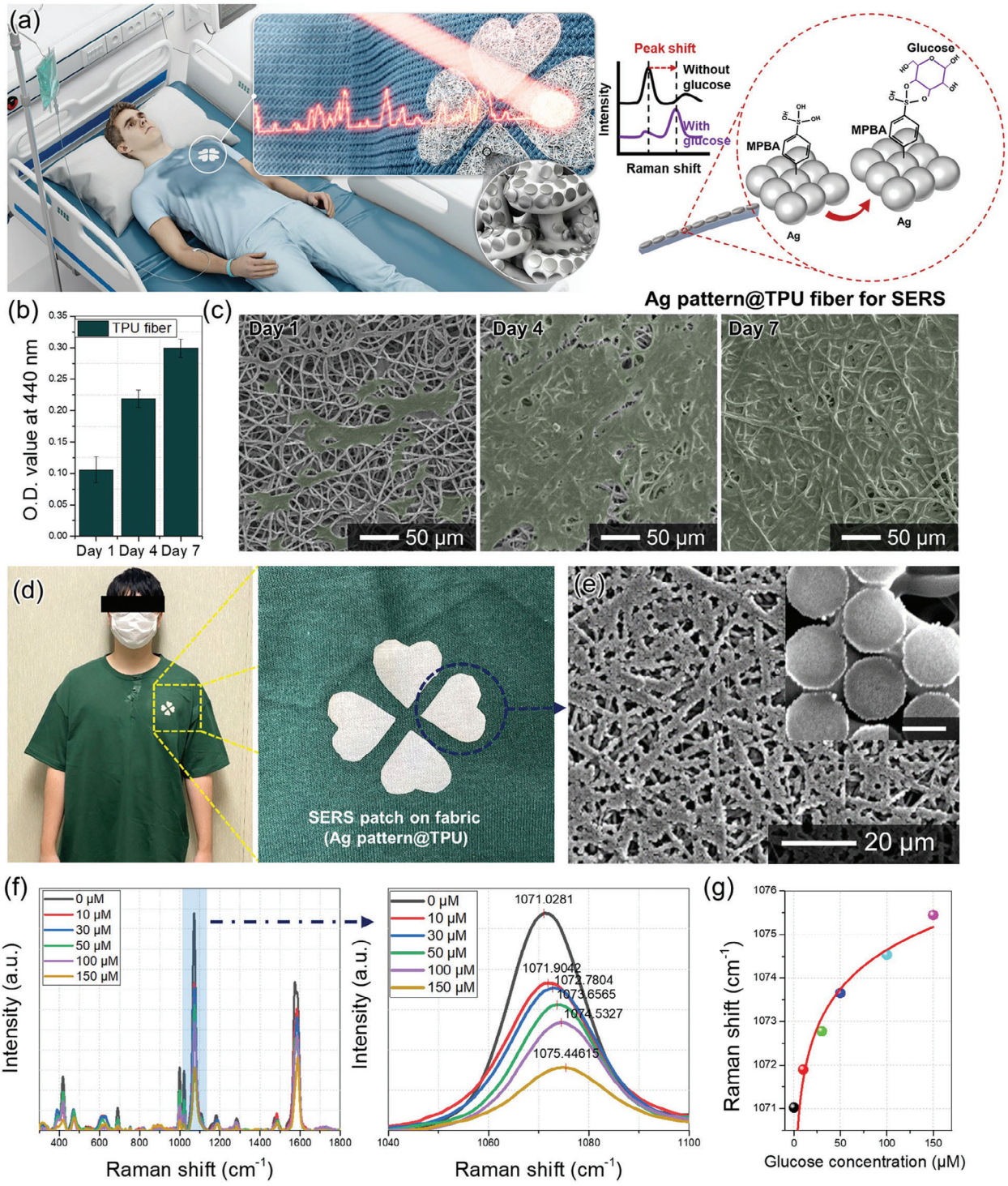


**Figure 4.** a) Illustration of the glucose level detection mechanism using SERS by the electrospun TPU fibers including 4-MPBA-immobilized silver circular patterns. The Raman peak shift is generated due to the vibrating structure change by the integration of 4-MPBA-glucose. The suggested SERS patch-based wearable diagnosable garment concept is depicted. b) Cell proliferation results to verify the biocompatibility of the electrospun TPU fibers for 7 days are shown. c) SEM images of cell proliferation morphologies on the electrospun TPU fibers for 7 days are observed (Green area: cell growth regions). d) Photographic image showing a demo of garment integrating 4-MPBA-immoblized silver patterns transferred electrospun TPU-based SERS patch. e) Morphological properties of the Ag circular patterns/TPU system, as examined by SEM (inset image scale bar: 1 μm) f) SERS results obtained for the Ag circular patterns/TPU systems at different glucose concentrations. The Raman peak (1071.0 $cm^{-1}$) of the control shifted to 1075.4 $cm^{-1}$ upon increasing the glucose concentration to 150 μM. (g) Tendency of Raman shift change according to the glucose concentration (i.e., 0, 10, 30, 50, 100, and 150 μM).

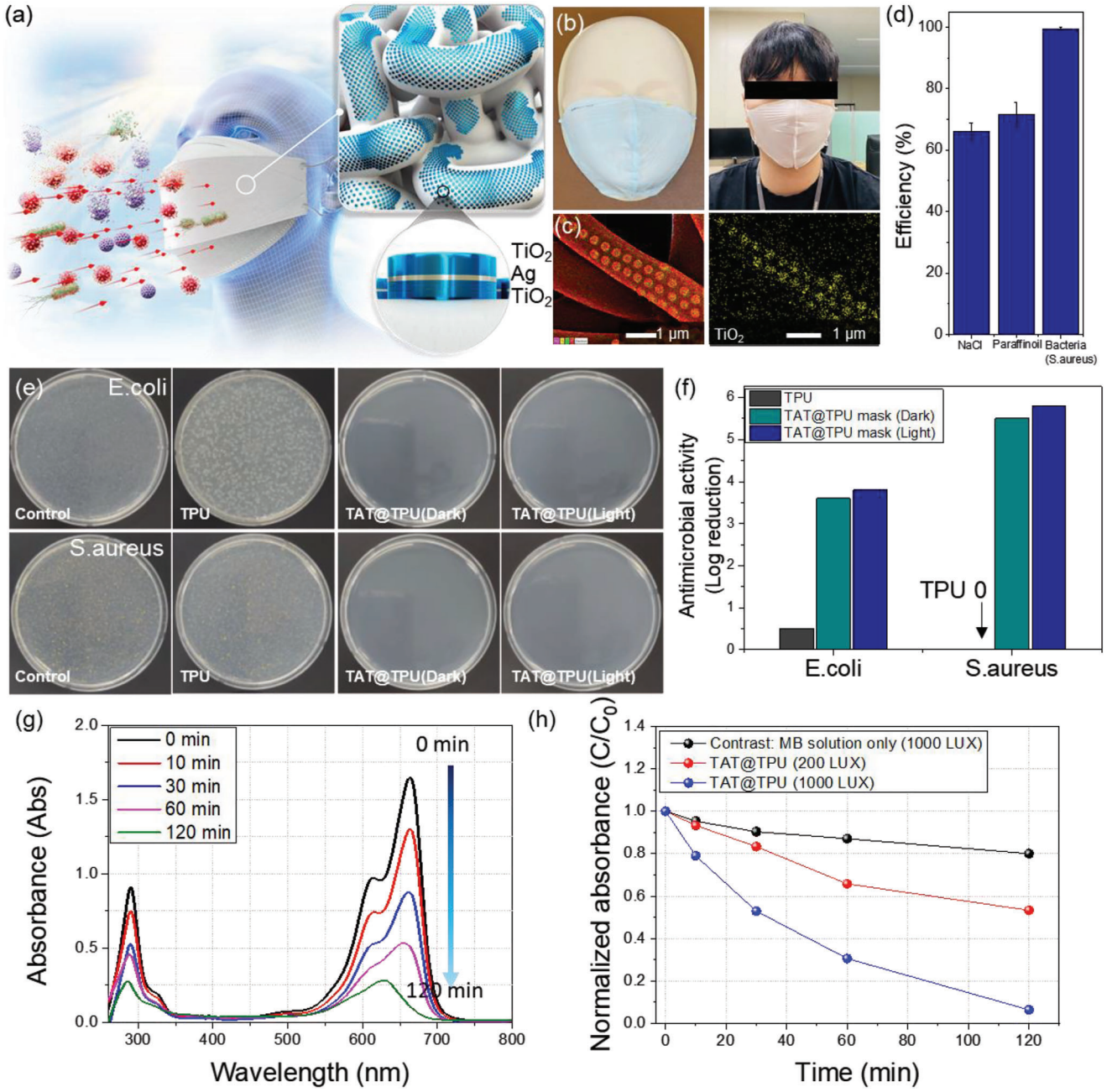


**Figure 5.** a) Mechanism of action of the TAT@TPU-based bactericidal mask. b) Photographic image of the TAT@TPU-based mask being worn. c) EDS images of TAT nanodot pattern on the electrospun TPU fiber. d) Filtration efficiency of the electrospun TPU mask against NaCl, paraffin oil, and bacteria (*S. aureus*). e) Photographic images of the antimicrobial test results for the three cases outlined in part (d). f) Antimicrobial performance of the electrospun TPU-based composite for the electrospun TPU, TAT on the electrospun TPU (dark environment), and TAT on the electrospun TPU (light exposure at 200 lux). g) Photocatalytic degradation performance of MB by TAT@TPU. UV–vis analysis was conducted over the visible light range. Upon increasing the light exposure time, the intensity of the peak at 664 nm was reduced. h) Variation in the MB-normalized absorbance ($C/C_0$) for TAT@TPU (200 lux), TAT@TPU (1000 lux), and the control over time.

TPU(TAT@TPU) mask was specifically engineered to enhance its antimicrobial efficacy for everyday mask usage through visible light irradiation. This approach was rooted in the anticipation of a synergistic interaction between the antimicrobial and BFE attributes of the TAT nanopatterns and the electrospun TPU fibers. Figure 5e shows the antimicrobial test results obtained for the TPU, TAT@TPU (without light), and TAT@TPU (with light) specimens against *Escherichia coli* (*E. coli*, Gram-positive) and *S. aureus* (Gram-negative). In the case of the pure electrospun TPU, the microbial resistance was low, with log reduction values of 0.5 (67.9% antimicrobial activity) for *E. coli* and 0 (0% antimicrobial activity) for *S. aureus*, respectively. In contrast, the TAT@TPU

**Table 1.** Filtration efficiency of the electrospun TPU mask against NaCl, paraffin oil, and bacteria (*S. aureus*).

| Filtration material | Filtration efficiency [%] |
|---|---|
| NaCl | 66 |
| Paraffin oil | 71.6 |
| Bacteria (*S. aureus*) | 99.8 |

gave log reductions of 3.6 (99.9% antimicrobial activity) for *E. coli* and 5.5 (99.9% antimicrobial activity) for *S. aureus*, respectively, even in a dark environment owing to the antibacterial characteristics of $TiO_2$ and Ag (**Table 2**). Furthermore, upon visible light irradiation (200 lux), enhanced antibacterial effects were observed for the TAT@TPU material compared to those observed in the dark. More specifically, log reductions of 3.8 and 5.8 were observed for *E. coli* and *S. aureus*, respectively, representing a 99.9% antibacterial activity in both cases. Afterward, the capacity of TAT@TPU to effectively purify water under visible light exposure was assessed alongside its antimicrobial performance. Additionally, leveraging the TAT nanodots to augment the photocatalytic degradation characteristics of the developed system, the degradation of methylene blue (MB) using TAT@TPU was examined as a model for water pollution treatment. Figure S20 (Supporting Information) shows the experimental setup, wherein the TAT@TPU was continuously exposed to visible light using a solar illuminator. As a result, the blue color of MB was faded by increasing light irradiation time (Figure S21, Supporting Information). For a quantitative analysis of the degree of dilution as a function of light irradiation time, UV–vis spectroscopy was employed to monitor the variation in the MB concentration (Figure 5g). It was found that upon increasing the exposure time to visible light, MB was successfully degraded and the blue color faded (i.e., the absorbance at 664 nm decreased). This suggests that the photocatalytic effect of the TAT nanopatterns led to the degradation of MB. Figure 5h shows the normalized results for the reduction in MB concentration over time for different samples. More specifically, it can be seen that after 120 min at 1000 lux of light illumination in the absence of $TiO_2$-based materials, the degree of MB degradation reached only 20%. In contrast, under the same light intensity, the presence of TAT@TPU resulted in a significant reduction in the concentration of MB (methylene blue). Specifically, the MB concentration decreased by 93.7% in the presence of TAT@TPU after 120 min. Furthermore, when exposed to even lower light intensity of 200 lux (equivalent to indoor fluorescent light), the photocatalytic degradation effect of TAT@TPU led to a degradation of MB reaching 46.7% after a duration of 120 min. These findings demonstrate the efficient photocatalytic activity of TAT@TPU in the degradation of MB under light irradiation. This indicates that masks exhibiting enhanced microbial resistance could be formulated by capitalizing on these photocatalytic degradation effects, potentially enabling the extended use of such masks without the need for frequent disinfection.

## 3. Conclusion

This study presented a new fabrication strategy for transferring M/MO NPs onto electrospun fibers using oxygen plasma treatment and heat pressing process. Utilizing this approach, the lateral etching of mold diminished the adhesive force between the mold and the nanopatterns. Furthermore, the formation of hydroxyl groups on the surface, reduction of surface energy, and mechanical interlocking by thermoforming characteristics enhanced the nanopatterns' adherence to the target substrate. The treatment time for surface modification, pressure, and temperature were optimized to enhance the quality of the transferred NPs. This optimized fabrication process has been employed to effectively transfer nanopatterns of diverse shapes and materials, including metals and metal oxides. The potential applications of the proposed M/MO NPs transferred onto electrospun TPU were demonstrated in two healthcare applications. First, a wearable SERS patch was developed for monitoring glucose levels in sweat, enabling the diagnosis and monitoring of hypoglycemia and diabetes. Second, a photocatalytic bactericidal mask was developed, which exhibited antimicrobial properties when exposed to visible light. It is important to highlight that while there have been prior studies involving the transfer of M/MO NPs onto flat polymer films or rigid substrates, the accomplishment of successful transfer onto electrospun fibers with a diameter of under 3 μm had not been previously reported. This underscores the distinctiveness of the proposed approach for transferring various M/MO NPs onto electrospun fibers. Furthermore, functional textiles based on electrospun fibers with these transferred nanopatterns are anticipated to be recyclable through the dissolution of the electrospun fibers and the separation of the nanopatterns. In summary, the capability to transfer a range of M/MO NPs onto electrospun fibers is anticipated to yield a wide array of industrial applications including sensors, flexible displays, wearable systems, and bio-applications.

## 4. Experimental Section

*Materials*: TPU was purchased from the WOOJIN Corporation (Korea). *N,N*-Dimethylformamide (DMF), and dichloromethane were purchased from Duksan Chemical (Korea). The metal (Au, Ag, Al, and Ni) and metal oxide ($TiO_2$ and $SiO_2$) sources were purchased from TAEWON SCIENTIFIC CO., LTD.(Korea).

*Fabrication*: To prepare TPU solutions, different weight percentages (5, 10, 15, or 20 wt.%) of TPU were dissolved in a mixture of dimethylformamide and dichloromethane (1:1, v/v) using uniform magnetic stirring at 500 rpm for 4 h. The TPU microfibers were fabricated using an electrospinning system from NANO NC Co., Ltd. (Korea) under a relative humidity of 34%. During the electrospinning process, the input power was set to 20 kV, and the distance between the needle tip and the collector was maintained at 15 cm.

For the preparation of the M/MO NPs, PUA resin (311-RM, Munuta Tech. Co., Ltd., Kore) was poured onto a nanopatterned master wafer and uniformly pushed using a roller. The PUA-based mold was then cured by irradiation with UV light for 3 min. After curing the PUA mold, metal or metal oxide layer (thickness: 30 nm) was deposited using an e-beam evaporator (Daeki Hi-Tech Co., Ltd., Korea, Vacuum pressure of≈10–6 Torr). The base mold of M/MO NPs was then etched and functionalized by oxygen plasma treatment for 5 min (treatment times of 1, 3, and 10 min were also used for comparison). The pure electrospun TPU was also treated with oxygen plasma for 5 min for comparative experiments. The power applied and flow rate of $O_2$ during plasma treatment were 100 W and 50 sccm, respectively. After the plasma treatment, the nanopattern mold was thermally pressed on the electrospun TPU at 100 °C and at a pressure of 5 bars for 5 min. For comparison, nanopattern transfer on to electrospun fibers was performed at pressures of 1, 3, 7, and 8 bar and temperatures of 50,

**Table 2.** Antimicrobial properties of the TPU, TAT@TPU (dark), and TAT@TPU (light) systems against *E. coli* and *S. aureus*.

| | *E. coli* reduction [log] | Reduction rate [%] | *S. aureus* reduction [log] | Reduction rate [%] |
|---|---|---|---|---|
| TPU | 0.0 | 0 | 0.5 | 67.9 |
| TAT@TPU (dark) | 5.5 | 99.9 | 3.6 | 99.9 |
| TAT@TPU (light) | 5.8 | 99.9 | 3.8 | 99.9 |

75, 125, and 150 °C. Finally, the mold was removed from the electrospun TPU.

*Characterization*: Morphological analysis was performed using ultra high resolution FE-SEM (Hitachi High-Technologies Corp, SU8230). The elements in the prepared M/MO@TPU specimen were analyzed by EDS (Hitachi High-Technologies Corp, SU8230; scan time = 100 s). The WCAs of the electrospun TPU and the metal-deposited nonpatterns were measured using 5 µL droplet with a water contact analysis equipment (KRÜSS Scientific). FTIR analysis (range = 4000–400 $cm^{-1}$) was conducted for the electrospun TPU using an FTIR spectrometer (Thermo Fisher Scientific, Nicolet iS50). FIB milling and SEM observations were conducted using a FIB-SEM instrument (Hitachi High-Technologies Corp, FB-2100). The mechanical properties were evaluated using a universal testing machine (Shimadzu, AGS-X). Sweat-wetted samples were prepared by immersing the nanopattern-transferred electrospun TPU in artificial perspiration (TMABIO, pH 5.5, ISO 105-B07). XPS analysis of electrospun TPU and electrospun TPU with Au nanopatterns transferred was performed using a Nexsa G2 instrument from Thermo Scientific. The mechanical properties of electrospun TPU with transferred nanopatterns, both dry and immersed in artificial sweat, were evaluated using a universal testing machine (AGS-X, Shimadzu).

*SERS Experiments*: To determine the glucose concentration in sweat, a Ag-transferred electrospun TPU patch was prepared by the abovementioned fabrication process. After the patch fabrication, it was submerged in a solution of MPBA for 1 day to functionalize the Ag component for glucose detection. Subsequently, glucose solutions of various concentrations (10–150 µM) were dropped onto the patch, and SERS analysis was carried out using a Raman Spectroscopy system (Horiba Jobin Yvon, ARAMIS) for glucose detection. The Raman shift range was set at 300–1800 $cm^{-1}$, and a 633 nm laser was employed for analysis.

*Mask Filtration Efficiency*: An electrospun TPU-based mask was fabricated using heat pressing method at 100 °C and a pressure of 5 bars for 5 min. The filtration efficiency of the electrospun TPU-based mask toward NaCl, paraffin oil, and bacteria (i.e., the bacterial filtration efficiency, BFE) was determined using 10 electrospun TPU sheets with a size of 15 cm × 15 cm. The efficiency for NaCl and paraffin oil was calculated using Equation (2), while the BFE was calculated using Equation (3), as follows:

$$P\,(\%) = \frac{C_1 - C_2}{C_1} \times 100 \tag{2}$$

Where P is the filtration efficiency, and $C_1$ and $C_2$ are the concentrations of NaCl or paraffin oil before and after passing through the mask sheet, respectively.

$$B\,(\%) = \frac{(C - T)}{C} \times 100 \tag{3}$$

where B is the bacterial filtration efficiency (%), C is the average number of bacterial colonies in the positive control group, and T is the total number of bacterial colonies in the test group.

*Antimicrobial Activity*: The antimicrobial efficacy of the developed mask textile against *E. coli* and *S. aureus* was verified according to the JIS Z 2801 standard method. A liquid culture medium (nutrient agar plate: Bacto-Peptone, 5 g; beef extract, 3 g; deionized water, 1000 mL) was used for microbial growth. Nutrient agar was sterilized by autoclaving ($10^3$ kPa and 120 °C). The microbes were cultivated in a nutrient agar medium (10 mL) at 37 ± 1 °C for 24–48 h. The samples were then cultivated with three control test specimens and three processed samples for 18 h in a glass container. All flat media were cultured at 37 ± 1 °C for 24–48 h, and after incubation, the number of colonies in a Petri dish containing 30–300 colonies of probiotic water were counted and recorded. The number of live microbes (M) was calculated using Equation (4):

$$M = Z \times R \times 20 \tag{4}$$

Where Z is the number of colonies, R is the dilution factor, and 20 represents the amount (ml) of saline. The antimicrobial reduction rates were calculated using Equation (5):

$$\log M_a - \log M_c \tag{5}$$

where $M_a$ is the initial live microbial number in the control, and $M_c$ is the live microbial number after 18 h of incubation.

*Photocatalytic Degradation of MB*: The MB solution was prepared using DI water (100 mL) and MB powder (0.05 g) by magnetic stirrer for 4 h. The MB solution was then poured into a vial containing TAT@TPU. Visible light (at 200 and 1000 lux) was used to irradiate the MB solution using a solar illuminator. The photocatalytic degradation test was conducted under various time conditions (i.e., 0, 10, 30, 60, and 120 min), and at each time point, the MB concentration was analyzed by UV–vis spectroscopy over a wavelength range of 250–800 nm.

## Acknowledegements

J.-H.H. and J.K. contributed equally to this work. This work was supported by the National Research Foundation of Korea (NRF) grant funded by the Korean government (MSIT, No. 2021R1A2C3008742); Alchemist Project grant funded by the Korea Evaluation Institute of Industrial Technology (KEIT) & the Korea Government (MOTIE) (Project Number: 1415179744, 20019169).

## Supporting Information

Supporting Information is available from the Wiley Online Library or from the author.

## Conflict of Interest

The authors declare no conflict of interest.

## Data Availability Statement

The data that support the findings of this study are available from the corresponding author upon reasonable request.

## Keywords

bactericidal mask, functional textile, nanotransfer printing, sweat monitoring, wearable healthcare

Received: January 24, 2024
Revised: March 19, 2024
Published online:

[1] K. Wilson, *A History of Textiles*, Routledge, New York **2021**.
[2] Z. Zhang, D. Ji, H. He, S. Ramakrishna, *Mater. Sci. Eng., R* **2021**, *143*, 100594.
[3] N. A. Patil, P. M. Gore, N. Jaya Prakash, P. Govindaraj, R. Yadav, V. Verma, D. Shanmugarajan, S. Patil, A. Kore, B. Kandasubramanian, *Chem. Eng. J.* **2021**, *416*, 129152.
[4] Y. Cheng, C. Wang, J. Zhong, S. Lin, Y. Xiao, Q. Zhong, H. Jiang, N. Wu, W. Li, S. Chen, B. Wang, Y. Zhang, J. Zhou, *Nano Energy* **2017**, *34*, 562.
[5] H. W. Choi, D. W. Shin, J. Yang, S. Lee, C. Figueiredo, S. Sinopoli, K. Ullrich, P. Jovančić, A. Marrani, R. Momentè, J. Gomes, R. Branquinho, U. Emanuele, H. Lee, S. Y. Bang, S. M. Jung, S. D. Han, S. Zhan, W. Harden-Chaters, Y. H. Suh, X. B. Fan, T. H. Lee, M. Chowdhury, Y. Choi, S. Nicotera, A. Torchia, F. M. Moncunill, V. G. Candel, N. Durães, K. Chang, et al., *Nat. Commun.* **2022**, *13*, 3528.
[6] K. Cherenack, C. Zysset, T. Kinkeldei, N. Münzenrieder, G. Tröster, *Adv. Mater.* **2010**, *22*, 5178.
[7] J. Shi, S. Liu, L. Zhang, B. Yang, L. Shu, Y. Yang, M. Ren, Y. Wang, J. Chen, W. Chen, Y. Chai, X. Tao, *Adv. Mater.* **2020**, *32*, 1901958.
[8] J. Ko, Z. J. Zhao, S. H. Hwang, H. J. Kang, J. Ahn, S. Jeon, M. Bok, Y. Jeong, K. Kang, I. Cho, J. H. Jeong, I. Park, *ACS Nano* **2020**, *14*, 2191.
[9] F. Marra, S. Minutillo, A. Tamburrano, M. S. Sarto, *Mater. Des.* **2021**, *198*, 109306.
[10] W. He, C. Wang, H. Wang, M. Jian, W. Lu, X. Liang, X. Zhang, F. Yang, Y. Zhang, *Sci. Adv.* **2019**, *5*, eaax0649.
[11] Y. Luo, Y. Li, P. Sharma, W. Shou, K. Wu, M. Foshey, B. Li, T. Palacios, A. Torralba, W. Matusik, *Nat. Electron.* **2021**, *4*, 193.
[12] J. Wei, X. Aeby, G. Nyström, *Adv. Mater. Technol.* **2023**, *8*, 2370002.
[13] J. Wei, C. Zhu, Z. Zeng, F. Pan, F. Wan, L. Lei, G. Nyström, Z. Fu, *Interdiscip. Mater.* **2022**, *1*, 495.
[14] J. Wei, J. Xie, P. Zhang, Z. Zou, H. Ping, W. Wang, H. Xie, J. Z. Shen, L. Lei, Z. Fu, *ACS Appl. Mater. Interfaces* **2021**, *13*, 2952.
[15] J. H. Ha, J. Y. Kim, D. Kim, J. Ahn, Y. Jeong, J. Ko, S. Hwang, S. Jeon, Y. Jung, J. Gu, H. Han, J. Choi, G. Lee, M. Bok, S. A. Park, Y. S. Cho, J. H. Jeong, I. Park, *Adv. Mater. Technol.* **2023**, *8*, 2201765.
[16] S. H. Jeong, Y. Lee, M. G. Lee, W. J. Song, J. U. Park, J. Y. Sun, *Nano Energy* **2021**, *79*, 105463.
[17] K. Meng, S. Zhao, Y. Zhou, Y. Wu, S. Zhang, Q. He, X. Wang, Z. Zhou, W. Fan, X. Tan, J. Yang, J. Chen, *Matter* **2020**, *2*, 896.
[18] A. Libanori, G. Chen, X. Zhao, Y. Zhou, J. Chen, *Nat. Electron.* **2022**, *5*, 142.
[19] T. Tat, G. Chen, X. Zhao, Y. Zhou, J. Xu, J. Chen, *ACS Nano* **2022**, *16*, 13301.
[20] N. Karim, S. Afroj, K. Lloyd, L. C. Oaten, D. V. Andreeva, C. Carr, A. D. Farmery, I. D. Kim, K. S. Novoselov, *ACS Nano* **2020**, *14*, 12313.
[21] J. Wei, Y. Yang, F. Pan, K. Yang, Y. Wang, Z. Zeng, Q. Wang, Z. Fu, *Compos. Part A Appl. Sci. Manuf.* **2023**, *172*, 107626.
[22] T. Liu, R. Liang, H. He, Y. Zeng, Z. Hou, Y. Liu, J. Yuan, B. Luo, S. Zhang, C. Cai, S. Wang, D. Lu, S. Nie, *Nano Energy* **2023**, *112*, 108480.
[23] Z. Zhou, S. Padgett, Z. Cai, G. Conta, Y. Wu, Q. He, S. Zhang, C. Sun, J. Liu, E. Fan, K. Meng, Z. Lin, C. Uy, J. Yang, J. Chen, *Biosens. Bioelectron.* **2020**, *155*, 112064.
[24] X. He, S. Yang, Q. Pei, Y. Song, C. Liu, T. Xu, X. Zhang, *ACS Sens* **2020**, *5*, 1548.
[25] Z. Li, J. Cheng, X. Yang, H. Liu, X. Xu, L. Ma, S. Shang, Z. Song, *Int. J. Biol. Macromol.* **2020**, *150*, 1.
[26] R. Bengalli, A. Colantuoni, I. Perelshtein, A. Gedanken, M. Collini, P. Mantecca, L. Fiandra, *NanoImpact* **2021**, *21*, 100282.
[27] T. Busolo, P. K. Szewczyk, M. Nair, U. Stachewicz, S. Kar-Narayan, *ACS Appl. Mater. Interfaces* **2021**, *13*, 16876.
[28] S. Ghosh, B. Nitin, S. Remanan, Y. Bhattacharjee, A. Ghorai, T. Dey, T. K. Das, N. C. Das, *ACS Appl. Mater. Interfaces* **2020**, *12*, 17988.
[29] J. Ahn, J. Gu, B. Hwang, H. Kang, S. Hwang, S. Jeon, J. Jeong, I. Park, *Nanotechnology* **2019**, *30*, 455707.
[30] L. Wang, M. Zhang, B. Yang, J. Tan, *ACS Appl. Mater. Interfaces* **2021**, *13*, 41933.
[31] S. Lepak-Kuc, B. Podsiadły, A. Skalski, D. Janczak, M. Jakubowska, A. Lekawa-Raus, *Nanomaterials* **2019**, *10*, 9.
[32] Y. Yang, B. Xu, Y. Gao, M. Li, *ACS Appl. Mater. Interfaces* **2021**, *13*, 49927.
[33] Y. Wu, X. Dai, Z. Sun, S. Zhu, L. Xiong, Q. Liang, M. C. Wong, L. B. Huang, Q. Qin, J. Hao, *Nano Energy* **2022**, *98*, 107240.
[34] M. Duan, X. Wang, W. Xu, Y. Ma, J. Yu, *ACS Appl. Mater. Interfaces* **2021**, *13*, 57943.
[35] A. Nandakumar, R. Truckenmüller, M. Ahmed, F. Damanik, D. R. Santos, N. Auffermann, J. De Boer, P. Habibovic, C. Van Blitterswijk, L. Moroni, *Small* **2013**, *9*, 3405.
[36] Y. Shao, G. Du, B. Luo, T. Liu, J. Zhao, S. Zhang, J. Wang, M. Chi, C. Cai, Y. Liu, X. Meng, Z. Liu, S. Wang, S. Nie, *Adv. Mater.* **2024**, 2311993.
[37] J. Wei, F. Pan, H. Ping, K. Yang, Y. Wang, Q. Wang, Z. Fu, *Research* **2023**, *6*, 0164.
[38] J. Ahn, J. Ha, Y. Jeong, Y. Jung, J. Choi, J. Gu, S. H. Hwang, M. Kang, J. Ko, S. Cho, H. Han, K. Kang, J. Park, S. Jeon, J. Jeong, I. Park, *Nat. Commun.* **2023**, *14*, 833.
[39] H. J. Lee, D. J. Shin, K. Park, *J. Mech. Sci. Tech.* **2017**, *31*, 5687.
[40] M. O. H. Cioffi, H. J. C. Voorwald, R. P. Mota, *Mater. Charact.* **2003**, *50*, 209.
[41] Y. J. Shin, Y. Wang, H. Huang, G. Kalon, A. T. S. Wee, Z. Shen, C. S. Bhatia, H. Yang, *Langmuir* **2010**, *26*, 3798.
[42] Z. Yang, H. Peng, W. Wang, T. Liu, *J. Appl. Polym. Sci.* **2010**, *116*, 2658.
[43] Q. Yuan, T. Zhou, L. Li, J. Zhang, X. Liu, X. Ke, A. Zhang, *RSC Adv.* **2015**, *5*, 31153.
[44] B. Lan, P. Li, X. Luo, H. Luo, Q. Yang, P. Gong, *Polymer* **2021**, *212*, 123159.
[45] M. Chi, S. Zhang, T. Liu, Y. Liu, B. Luo, J. Wang, C. Cai, X. Meng, S. Wang, Q. Duan, S. Nie, *Adv. Funct. Mater.* **2023**, *34*, 2310280.
[46] A. L. Giraldo-Aguirre, E. D. Erazo-Erazo, O. A. Flórez-Acosta, E. A. Serna-Galvis, R. A. Torres-Palma, *J. Photochem. Photobiol A Chem.* **2015**, *311*, 95.
[47] S. R. Zavalkoff, C. Polychronakos, *Diabetes Care* **2002**, *25*, 1603.
[48] Z. Wang, J. Shin, J. H. Park, H. Lee, D. H. Kim, H. Liu, *Adv. Funct. Mater.* **2021**, *31*, 2008130.
[49] Y. J. Hong, H. Lee, J. Kim, M. Lee, H. J. Choi, T. Hyeon, D. H. Kim, *Adv. Funct. Mater.* **2018**, *28*, 1805754.
[50] M. A. Zahed, M. Sharifuzzaman, H. Yoon, M. Asaduzzaman, D. K. Kim, S. Jeong, G. B. Pradhan, Y. Do Shin, S. H. Yoon, S. Sharma, S. Zhang, J. Y. Park, *Adv. Funct. Mater.* **2022**, *32*, 2208344.
[51] Q. Yuan, H. Fang, X. Wu, J. Wu, X. Luo, R. Peng, S. Xu, S. Yan, *ACS Appl. Mater. Interfaces* **2023**.
[52] Y. Qin, J. Mo, Y. Liu, S. Zhang, J. Wang, Q. Fu, S. Wang, S. Nie, *Adv. Funct. Mater.* **2022**, *32*, 2201846.

[53] R. S. André, C. A. Zamperini, E. G. Mima, V. M. Longo, A. R. Albuquerque, J. R. Sambrano, A. L. Machado, C. E. Vergani, A. C. Hernandes, J. A. Varela, E. Longo, *Chem. Phys.* **2015**, *459*, 87.
[54] A. Maurya, P. Chauhan, A. Mishra, A. K. Pandey, *J. Res. Updates Polym. Sci.* **2012**, *1*, 43.
[55] C. Xu, G. P. Rangaiah, X. S. Zhao, *Ind. Eng. Chem. Res.* **2014**, *53*, 14641.
[56] M. Xu, Y. Wang, J. Geng, D. Jing, *Chem. Eng. J.* **2017**, *307*, 181.
[57] D. Sarkar, C. K. Ghosh, S. Mukherjee, K. K. Chattopadhyay, *ACS Appl. Mater. Interfaces* **2013**, *5*, 331.